

Layer-Specific Developmentally Precise Axon Targeting of Transient Suppressed-by-Contrast Retinal Ganglion Cells

Nai-Wen Tien,^{1,2*} Carmela Vitale,^{1*} Tudor C. Badea,^{3,4,5} and Daniel Kerschensteiner^{1,6,7,8}

¹Department of Ophthalmology and Visual Sciences, Washington University School of Medicine, Saint Louis, Missouri 63110, ²Graduate Program in Neuroscience, Washington University School of Medicine, Saint Louis, Missouri 63110, ³Retinal Circuit Development and Genetics Unit, Neurobiology-Neurodegeneration and Repair Laboratory, National Eye Institute, Bethesda, Maryland 20892, ⁴Research and Development Institute, Transilvania University of Braşov, Braşov 500484, Romania, ⁵National Center for Brain Research, Research Institute for Artificial Intelligence, Romanian Academy, Cluj-Napoca 400293, Romania, ⁶Departments of Neuroscience and , ⁷Biomedical Engineering, Washington University School of Medicine, Saint Louis, Missouri 63110, and ⁸Hope Center for Neurological Disorders, Washington University School of Medicine, Saint Louis, Missouri 63110

The mouse retina encodes diverse visual features in the spike trains of >40 retinal ganglion cell (RGC) types. Each RGC type innervates a specific subset of the >50 retinorecipient brain areas. Our catalog of RGC types and feature representations is nearing completion. Yet, we know little about where specific RGC types send their information. Furthermore, the developmental strategies by which RGC axons choose their targets and pattern their terminal arbors remain obscure. Here, we identify a genetic intersection (*Cck-Cre* and *Brn3c^{CKOAP}*) that selectively labels transient Suppressed-by-Contrast (tSbC) RGCs, a member of an evolutionarily conserved functionally mysterious RGC subclass. We find that tSbC RGCs selectively innervate the dorsolateral geniculate nucleus (dLGN) and ventrolateral geniculate nucleus (vLGN) of the thalamus, the superior colliculus (SC), and the nucleus of the optic tract (NOT) in mice of either sex. They binocularly innervate dLGN and vLGN but project only contralaterally to SC and NOT. In each target, tSbC RGC axons occupy a specific sublayer, suggesting that they restrict their input to specific circuits. The tSbC RGC axons span the length of the optic tract by birth and remain poised there until they simultaneously innervate their four targets around postnatal day 3. The tSbC RGC axons choose the right targets and establish mature stratification patterns from the outset. This precision is maintained in the absence of *Brn3c*. Our results provide the first map of SbC inputs to the brain, revealing a narrow target set, unexpected laminar organization, target-specific binocularity, and developmental precision.

Key words: axon development; binocular; laminar targeting; retinal projections; thalamus

Significance Statement

In recent years, we have learned a lot about the visual features encoded by RGCs, the output neurons of the eye. In contrast, we know little about where RGCs send their information and how RGC axons, which carry this information, target specific brain areas during development. Here, we develop an intersectional strategy to label a unique RGC type, the tSbC RGC, and map its projections. We find that tSbC RGC axons are highly selective. They innervate few retinal targets and restrict their arbors to specific sublayers within these targets. The selective tSbC RGC projection patterns develop synchronously and without trial and error, suggesting molecular determinism and coordination.

Received Nov. 25, 2021; revised July 2, 2022; accepted July 8, 2022.

Author contributions: N-W.T., C.V., T.C.B., and D.K. designed research; N-W.T., C.V., and D.K. performed research; N-W.T., C.V., and D.K. analyzed data; and D.K. wrote the paper.

This work was supported by National Institutes of Health Grants EY027411 (D.K.), EY023341 (D.K.), EY026978 (D.K.), and EY034001 (D.K.); the Grace Nelson Lacy Research Fund (D.K.); Research to Prevent Blindness Unrestricted Grant 100001818 (Department of Ophthalmology and Visual Sciences); and Unitatea Executiva pentru Finantarea Invatamantului Superior, a Cercetarii, Dezvoltarii si Inovarii Grant PN-III-P4-PCE-2021-0333 (T.C.B.).

N.-W. Tien's present address: Spatial Navigation and Memory Unit, National Institutes of Health, Bethesda, Maryland.

*N-W.T. and C.V. share first authorship.

The authors declare no competing financial interests.

Correspondence should be addressed to Daniel Kerschensteiner at kerschensteiner@wustl.edu or Tudor C. Badea at badeatc@unitbv.ro.

<https://doi.org/10.1523/JNEUROSCI.2332-21.2022>

Copyright © 2022 the authors

Introduction

Vision begins in the retina, which transforms the pixel representations of photoreceptors into feature representations of retinal ganglion cells (RGCs), the sole output neurons of the eye (Gollisch and Meister, 2010; Kerschensteiner, 2022). The mouse retina contains >40 RGC types, which send different visual information to the brain (Baden et al., 2016; Bae et al., 2018; Rheaume et al., 2018; Tran et al., 2019; Goetz et al., 2022). We have learned a lot about how retinal circuits extract visual features and encode them in spike trains of specific RGC types (Kerschensteiner, 2022). Yet, we know little about where this information is sent.

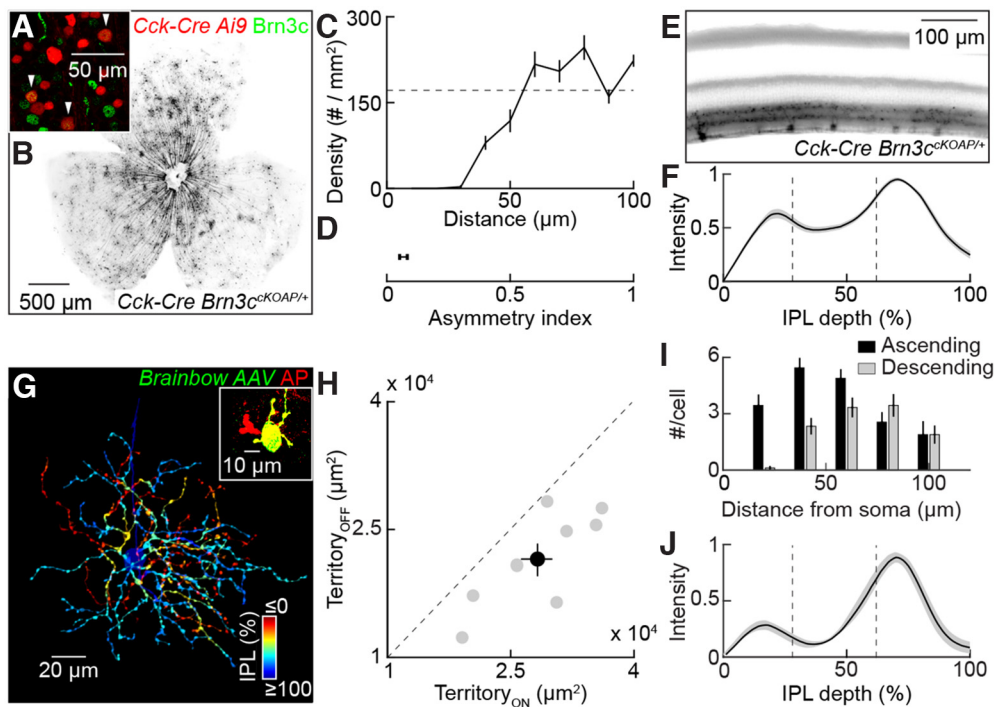


Figure 1. *Cck-Cre Brn3c^{CKOAP/+}* mice selectively labeled tSbC RGCs. **A**, Excerpt of a flat-mounted P30 *Cck-Cre Ai9* (red) retina stained for Brn3 (green). Arrowheads highlight double-positive cells. **B**, Retinal whole mount from a P30 *Cck-Cre Brn3c^{CKOAP/+}* mouse. **C**, DRP of RGCs labeled in P30 *Cck-Cre Brn3c^{CKOAP/+}* mice. Line indicates the mean, and error bars indicate SEM ($n = 10$ retinas). The dashed line indicates the average cell density and the expected profile for randomly distributed cells. **D**, Asymmetry index for the distribution of labeled RGCs in the four retinal quadrants (see above, Materials and Methods; $n = 5$ retinas). **E**, Vibratome slices through a 30 *Cck-Cre Brn3c^{CKOAP/+}* retina. **F**, Labeling profile across the IPL depth (i.e., RGC dendritic stratification profile) in P30 *Cck-Cre Brn3c^{CKOAP/+}* mice. Line indicates the mean, and shaded areas indicate SEM ($n = 10$ retinas). **G**, Orthogonal projections of a confocal image stack through a representative tSbC-RGC labeled by Brainbow AAV infection from a P30 *Cck-Cre Brn3c^{CKOAP/+}* mouse. The fluorescent signal is colored to represent depth in the IPL. Inset, Magnification of the soma, showing that the labeling of Brainbow AAV infection (green) overlaps with SEAP staining (red). **H**, Scatter plot of ON versus OFF dendritic territories. Gray dots show data from individual cells ($n = 9$), and the black circle with error bars indicates the mean and \pm SEM of the population. **I**, Histogram of the number of ascending and descending branches as a function of distance from the soma ($n = 9$). Error bars indicate \pm SEM. **J**, Dendritic stratification profile through the IPL. Dashed lines indicate IPL edges. Line indicates the mean, and shaded areas indicate \pm SEM ($n = 9$).

In total, mouse RGCs innervate >50 brain areas (Morin and Studholme, 2014; Martersteck et al., 2017). However, which brain areas specific RGC types innervate remains, with few exceptions, unknown (Hattar et al., 2006; Huberman et al., 2008, 2009; Kim et al., 2008; Yonehara et al., 2008). Some RGC axons target distinct layers within the dorsolateral geniculate nucleus (dLGN) and superior colliculus (SC), the two largest retinorecipient areas of the mouse brain (Reese, 1988; Huberman et al., 2009; Kim et al., 2010; Hong et al., 2011; Kerschensteiner and Guido, 2017). Our maps of RGC axons in dLGN and SC are incomplete, and the retinal input organization of many other targets remains unexplored. Finally, a subset of RGCs (9/40+ types) innervate ipsilateral and contralateral brain areas to support binocular vision (Dräger and Olsen, 1980; Johnson et al., 2021). Whether these RGC types innervate all or only a subset of their targets binocularly is unclear.

Retinal projections to the brain serve as a model for studying the development of long-range neural projections and supported the discovery of conserved growth programs and molecular cues that guide RGC axons toward their targets (Erskine and Herrera, 2007; Moore and Goldberg, 2011; Mason and Slavi, 2020; Williams et al., 2020). Yet, how RGC axons invade specific targets and organize their arbors within, and whether this process involves trial and error or proceeds orderly, is unknown (Kim et al., 2010; Osterhout et al., 2011, 2014, 2015; Su et al., 2021). Individual RGCs innervate multiple targets through axon collaterals to ensure

complete visual field representation in each retinorecipient area (Fernandez et al., 2016). Whether collaterals innervate targets simultaneously or sequentially is unclear (Osterhout et al., 2014). Brn3 POU domain transcription factors are part of the gene regulatory network that controls RGC specification and terminal identity (Mu and Klein, 2004; Badea et al., 2009). Brn3a, Brn3b, and Brn3c are expressed in distinct but overlapping sets of RGCs (Xiang et al., 1995; Badea and Nathans, 2011; Parmhans et al., 2018, 2021). RGC axon targeting is severely affected in *Brn3b* KO mice, but the contributions of Brn3a and Brn3c to this process remain to be tested (Badea et al., 2009, 2012).

Most RGCs increase their firing rates to light increments (i.e., positive contrast), light decrements (i.e., negative contrast), or both. However, Levick (1967) and Rodieck (1967) discovered RGCs in cats and rabbits, respectively, that fire at high rates in the absence of stimuli and are silenced by positive and negative contrast steps. Suppressed-by-Contrast (SbC) RGCs have since been identified in nonhuman primates and mice, indicating they are a conserved output of the mammalian retina (de Monasterio, 1978; Jacoby et al., 2015; Tien et al., 2015). The contributions of SbC signals to vision remain mysterious, in part because the projection patterns of SbC RGCs are unknown (Masland and Martin, 2007).

Here, we discover a genetic intersection that selectively labels transient SbC (tSbC) RGCs in mice. We use this intersection to map the tSbC RGC projections to the brain and study their development.

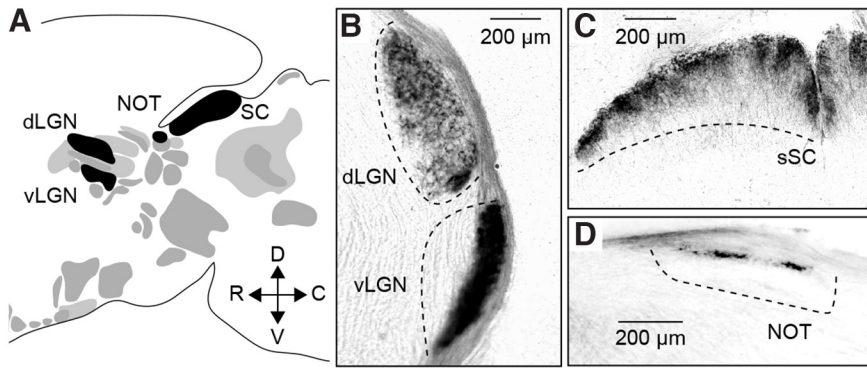


Figure 2. tSbC RGCs innervate four brain areas in a laminar-specific manner. **A**, Sagittal schematic view of the brain illustrating retinorecipient brain areas, with those innervated by tSbC RGCs painted black. **B–D**, Coronal sections of the LGN complex (**B**), SC (**C**), and NOT (**D**) of a P30 *Cck-Cre Brn3c^{CKOAP/+}* mouse showing the laminar-specific axonal targeting of tSbC RGCs.

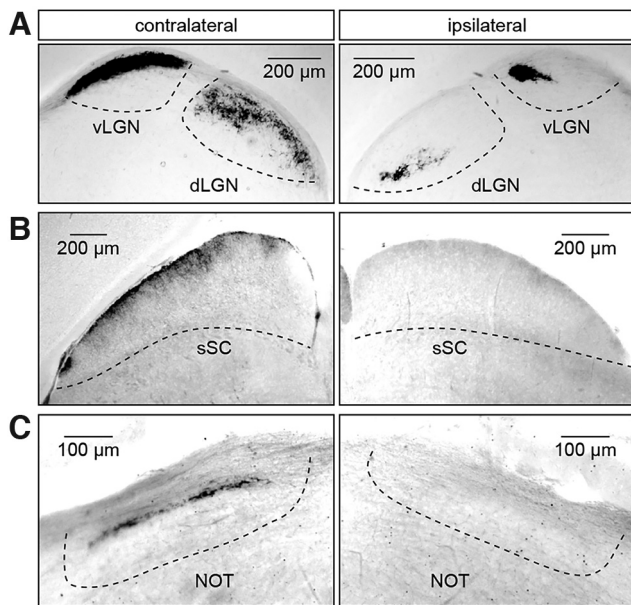


Figure 3. tSbC RGCs binocularly innervate a subset of their targets. **A–C**, Coronal sections of contralateral (left) and ipsilateral (right) LGN (**A**), SC (**B**), and NOT (**C**) 5 d after enucleation of a P30 *Cck-Cre Brn3c^{CKOAP/+}* mouse.

Materials and Methods

Experimental animals. We used the following mouse lines, alone or in combination: *Cck-Cre* (Taniguchi et al., 2011), *Brn3c^{CKOAP}* (Badea et al., 2012), and *Ai9* (Madisen et al., 2010). All mice were crossed onto a *C57Bl6/J* background for at least five generations before inclusion in this study. We used *Cck-Cre Brn3c^{CKOAP/CKOAP}* mice to test the contributions of *Brn3c* to the development of tSbC RGC projections. Although we did not independently confirm *Brn3c* deletion, we are confident that tSbC RGCs in these mice lack *Brn3c* because (1) alkaline phosphatase (AP) expression reports successful recombination and *Brn3c* excision, and (2) the recombined *Brn3c^{CKOAP}* allele has previously been used successfully as a null allele (Badea et al., 2012; Shi et al., 2013). Throughout our study, we used mice of both sexes, and because we observed no differences, combined their data.

Adeno-associated virus. A Brainbow adeno-associated virus (AAV; AAV-EF1a-BbTagBY, catalog #45185-AAV9, Addgene) was injected (250 nl) into the vitreous of newborn *Cck-Cre Brn3c^{CKOAP/+}* mice as described previously (Cai et al., 2013; Soto et al., 2013).

Tissue preparation and histochemistry. Tissues were either collected fresh or after transcardial perfusion. For fresh tissue collection, animals

were deeply anesthetized with CO₂, decapitated, and their retinas and brains collected. Retinas and brains were fixed by immersion in 4% paraformaldehyde (Sigma-Aldrich) for 30 min at room temperature and overnight at 4°C, respectively. For transcardial perfusions, animals were injected with ketamine (80 mg/kg) and xylazine (8 mg/kg) and perfused with ice-cold PBS followed by 4% paraformaldehyde (Sigma-Aldrich). Fixed brain and retina vibratome slices and fixed retinal whole mounts were washed twice for 20 min in PBS at room temperature. Before AP staining, brain sections and retinas in PBS were heated in a water bath at 65–70°C for 90 min to inactivate endogenous AP. AP staining was then developed in the heat-inactivated tissue in AP buffer (0.1 M Tris, 0.1 M NaCl, 50 mM MgCl₂, pH to 9.5) with 3.4 μl/ml of NBT/BCIP overnight at room temperature with gentle agitation (Badea et al., 2003). After staining, the tissue was washed three times for 20 min

in PBS with 0.1% Tween 20 and fixed overnight in PBS with 4% PFA at 4°C. To improve imaging, the tissue was dehydrated through an ethanol series (50, 75, 85, 95, and 100%, 100 proof, for 20 min, then 100%, 200 proof, overnight) and cleared with 2:1 Benzyl benzoate (BB)/Benzyl alcohol (BA). The tissue was then mounted in 2:1 BB/BA between glass slides and coverslips before the NBT/BCIP precipitate was dissolved in BB/BA. We used a rabbit polyclonal anti-*Brn3c* antibody (Xiang et al., 1995) to stain *Cck-Cre Ai9* retinas and a murine anti-secreted embryonic alkaline phosphatase (SEAP) antibody 0.03 mg/ml (VIB Core Protein) to stain *Cck-Cre Brn3c^{CKOAP/+}* retinas.

Imaging and analysis. We brightfield imaged the cleared tissue with 4× and 10× objectives on an Olympus BX51 microscope and a 2× objective on a Leica M205 FCA stereo microscope. We used an Olympus FV1000 laser-scanning confocal microscope with a 20× objective to analyze *Brn3c*-staining in *Cck-Cre Ai9* mice and a 60× objective to image AAV-Brainbow-positive cells and SEAP staining in *Cck-Cre Brn3c^{CKOAP/+}* mice. The dendritic territories, the ascending and descending branches, and the stratification profile were analyzed in image stacks with a voxel size of 0.207 μm (*x/y*-axis) to 0.5 μm (*z*-axis).

Density recovery profiles (DRPs) of labeled RGCs were calculated following the definitions of Rodieck (1991) using scripts written in MATLAB. RGC dendrite and axon stratification profiles were analyzed in Fiji (Schindelin et al., 2012). To determine whether labeled RGCs are regionally enriched or distributed evenly across the retina, we measured their density in four quadrants of each retina and defined an asymmetry index as follows:

$$\text{Asymmetry index} = \frac{(D_{\max} - D_{\min})}{(D_{\max} + D_{\min})},$$

where D_{\max} is the density of cells in the most populated quadrant, and D_{\min} is the density of cells in the least populated quadrant. Territories of ON and OFF dendrites were measured as the areas of the smallest convex polygons to encompass the respective arbors in maximum intensity projections. The distribution of ascending and descending branches was calculated as a function of the distance from the soma. The dendritic stratification profile was calculated as the mean fluorescent values of the tSbC RGCs as a function of distance normalized from the inner nuclear layer to the ganglion cell layer. Data were analyzed using Fiji and custom scripts written in MATLAB.

Results

An intersectional genetic strategy selectively labels tSbC RGC
We previously characterized tSbC RGCs in *Cck-Cre* transgenic mice injected with AAVs or crossed to a fluorescent reporter

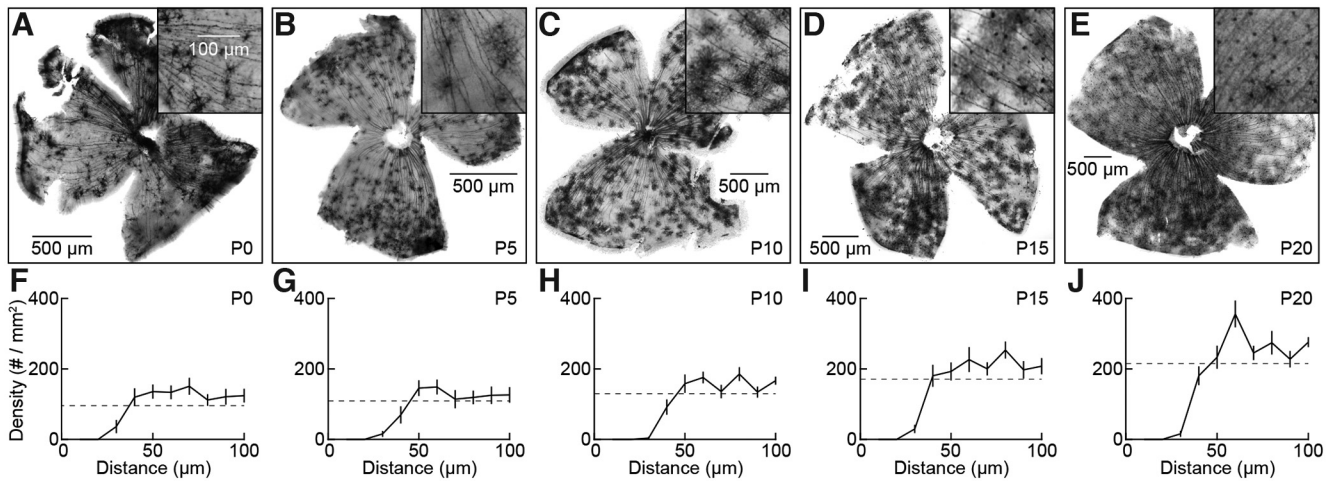


Figure 4. *Cck-Cre Brn3c^{CKOAP/+}* mice label tSbC RGCs throughout postnatal development. **A–E**, Representative whole mounts of *Cck-Cre Brn3c^{CKOAP/+}* retinas at P0 (**A**), P5 (**B**), P10 (**C**), P15 (**D**), and P20 (**E**). Insets, Magnified views of smaller regions at midcentricity. At P0 (**A**), some newborn tSbC RGCs that have not yet retracted their apical processes and completed migration to the ganglion cell layer are visible at the edges of the whole mounts (Sajgo et al., 2016). At all other ages (**B–E**), the AP labeling is restricted to tSbC RGCs in the ganglion cell layer. **F–J**, DRPs of labeled RGCs in *Cck-Cre Brn3c^{CKOAP/+}* retinas at P0 (**F**), P5 (**G**), P10 (**H**), P15 (**I**), and P20 (**J**); $n = 10$ retinas for each.

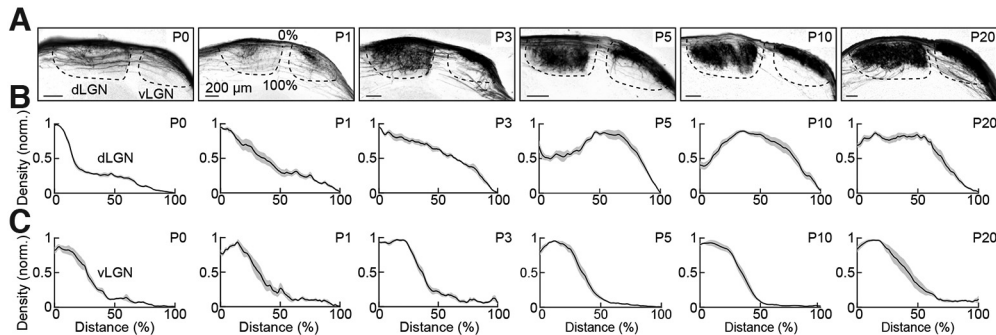


Figure 5. Development of the LGN innervation of tSbC RGC. **A**, Developmental time series of coronal sections through the LGN complex of *Cck-Cre Brn3c^{CKOAP/+}* mice (P0, P1, P3, P5, P10, P20, from left to right). **B, C**, Labeling profiles from the optic tract (0%) to the medial boundaries (100%) of dLGN (**B**) and vLGN (**C**) across development (P0, P1, P3, P5, P10, P20, from left to right). Lines indicate the mean, and shaded areas indicate SEM ($n = 3–5$ mice at each time point).

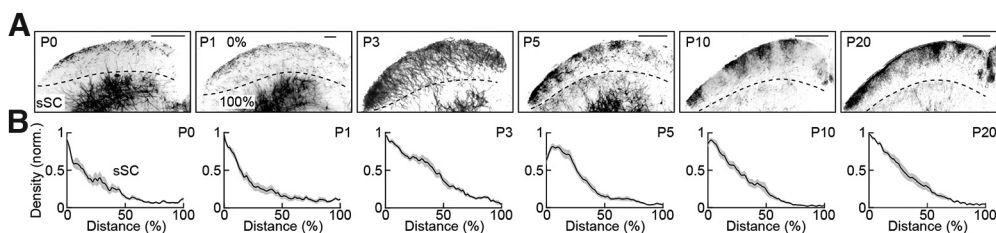


Figure 6. Development of the SC innervation of tSbC RGCs. **A**, Developmental time series of coronal sections through the SC of *Cck-Cre Brn3c^{CKOAP/+}* mice (P0, P1, P3, P5, P10, P20, from left to right). **B**, Labeling profiles from the surface of SC (0%) to the caudal margin of sSC (i.e., the caudal margin of the stratum opticum, 100%) across development (P0, P1, P3, P5, P10, P20, from left to right). Lines indicate the mean, and shaded areas indicate SEM ($n = 3–5$ mice at each time point).

strain (*Ai9*, tdTomato; Tien et al., 2015). In our previous characterization, we referred to these cells simply as SbC RGCs (Tien et al., 2015) because of their light responses, resemblance to SbC RGCs in rabbits (Levick, 1967; Sivyer et al., 2010), and because they were the only RGC type with SbC responses known in mice. Since then, two additional mouse SbC RGC types have been identified (Jacoby et al., 2015; Jacoby and Schwartz, 2018; Wienbar and Schwartz, 2022). These cells differ morphologically and functionally from the cell type we identified. One is suppressed for longer periods after contrast steps [i.e., sustained SBC (sSbC) RGC; Jacoby et al., 2015], and one fires action potentials in bursts [i.e., bursty SBC (bSbC) RGC; Wienbar

and Schwartz, 2022]. Following a change in nomenclature proposed by Jacoby et al. (2015), we now refer to the cell we originally identified as tSbC RGCs.

The bistratified dendrites of tSbC RGCs target synaptic laminae outside the inner plexiform layer (IPL) ChAT bands (i.e., the plexus of ON and OFF starburst amacrine cells) and are connected by numerous ascending and descending processes (Tien et al., 2015). An RGC type matching this morphologic description was reported in *Brn3c^{CKOAP/+}* mice crossed to a ubiquitously expressed sparsely induced Cre line (*R26CreERT* mice; Badaea and Nathans, 2011). Both *Cck-Cre Ai9* and *R26CreERT Brn3c^{CKOAP/+}* label multiple RGC types. To examine their

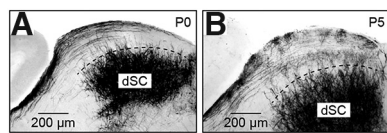


Figure 7. Labeling in *Cck-Cre Brn3c^{CKOAP/+}* sSC represents retinal axons. **A, B**, Sagittal sections through the SC of P0 and P5 *Cck-Cre Brn3c^{CKOAP/+}* mice. At these ages, neurons in dSC transiently express alkaline phosphatase. However, the neurites of dSC neurons are sparse in sSC, and most of the sSC labeling reflects axons entering from the optic tract (i.e., tSbC RGC axons).

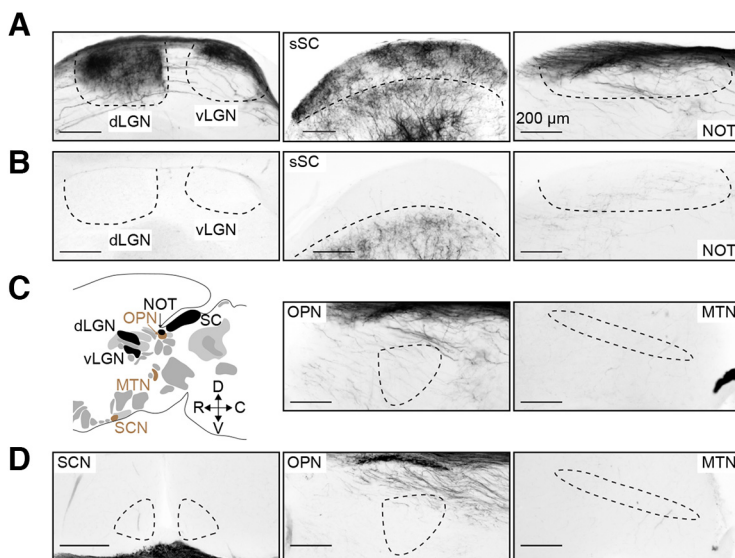


Figure 8. Developmental specificity of tSbC RGC target innervation. **A, B**, Coronal sections through the LGN complex (left), SC (middle), and NOT (right) in a P5 control mouse (**A**) and a P10 mouse, enucleated at P0 (**B**). **C, D**, Schematic (**C**, left) highlighting the position of exemplary retinorecipient targets omitted by tSbC RGCs during development (**C**, P5), and at maturity (**D**, P30) in *Cck-Cre Brn3c^{CKOAP/+}* mice.

overlap, we first stained *Cck-Cre Ai9* mice for *Brn3c*. This colabeled a set of uniformly sized RGC somata (Fig. 1A; 186 ± 16 cells/mm², $n = 6$ retinas). The colabeled cells made up $29.8 \pm 2.7\%$ of the *Brn3c*-positive and $17.0 \pm 1.3\%$ of the tdTomato-positive populations. We next crossed *Cck-Cre* and *Brn3c^{CKOAP/+}* mice. In mature *Cck-Cre Brn3c^{CKOAP/+}* mice postnatal day (P)30, a sparse population of RGCs (172 ± 7 cells/mm², $n = 10$ retinas) expressed alkaline phosphatase (Fig. 1B). The DRPs of the labeled RGCs showed pronounced exclusion zones (Fig. 1C), a hallmark of cell-type-specific retinal mosaics (Bae et al., 2018). Cells were distributed evenly across the retina (Fig. 1D). In vibratome slices, the labeled RGCs were consistently bistratified with dendrite arbors outside the expected ChAT band positions (Fig. 1E,F; Bae et al., 2018). To further confirm the identity of these cells, we injected a Brainbow AAV (*AAV-EF1a-BbTagBY*) intravitreally into *Cck-Cre Brn3c^{CKOAP/+}* mice, flat mounted retinas 4 weeks later, and stained them for AP. All AP-positive cells expressing the Cre-dependent Brainbow reporter/reporters (BFP, YFP, or both) showed characteristic morphologic features of tSbC RGCs (31/31 cells in three retinas), (1) bistratified dendrites stratifying outside the expected ChAT band positions, (2) smaller OFF than ON dendrite arbors, and (3) numerous ascending and descending processes connecting the ON and OFF arbors (Fig. 1G–J). No Brainbow-AAV-labeled cells of different morphology stained for AP (0/14 cells in three retinas). Finally, we found only two reporter-expressing cells (in three retinas) with tSbC RGC morphology that were AP

negative. Thus, *Cck-Cre Brn3c^{CKOAP/+}* mice label tSbC RGCs selectively and nearly completely.

tSbC RGCs innervate four brain areas in a layer-specific manner

To map the projections of tSbC RGCs, we cut coronal sections of *Cck-Cre Brn3c^{CKOAP/+}* mouse brains (P30) and stained them for alkaline phosphatase. Neurons in the brain did not express alkaline phosphatase. All brain labeling was eliminated by binocular enucleation (data not shown), indicating that it reflects the expression of alkaline phosphatase in tSbC RGC axons.

We comprehensively surveyed the retinorecipient areas of *Cck-Cre Brn3c^{CKOAP/+}* mouse brains (P30) and found labeling in only four (of >50; Morin and Studholme, 2014; Martersteck et al., 2017). In the LGN complex, the dLGN and ventrolateral geniculate nucleus (vLGN) were labeled, whereas the intergeniculate leaflet was clear (Fig. 2B). Labeling in dLGN encompassed all but the most medial aspect, and in vLGN, labeling was restricted to the most temporal layer (Fig. 2B). In SC, labeling was strongest in the upper layer of the retinorecipient superficial SC (sSC; Fig. 2C). Finally, we observed narrowly stratified labeling in the nucleus of the optic tract (NOT; Fig. 2D). Thus, tSbC RGC axons innervate a small subset of retinorecipient areas (4/50+) and target specific layers within each of these areas.

tSbC RGCs binocularly innervate a subset of their targets

We recently discovered that only nine of the >40 mouse RGC types innervate ipsilateral and contralateral brain areas to support binocular vision (Johnson et al., 2021). The remaining types innervate only contralateral targets. tSbC RGCs are part of the ipsilaterally projecting set (Johnson et al., 2021). To test whether tSbC RGCs innervate all their targets binocularly, we examined alkaline phosphatase labeling in the brains of monocularly enucleated *Cck-Cre Brn3c^{CKOAP/+}* mice. We enucleated mice at P25 and analyzed RGC projection patterns at P30 to allow for Wallerian degeneration of RGC axons from the removed eye (Knöferle et al., 2010). All four targets received contralateral tSbC RGC input (Fig. 3A–C), but only the dLGN and vLGN received input from ipsilateral tSbC RGCs (Fig. 3A). Thus, tSbC RGCs binocularly innervate only a subset of their targets, the first example of target-specific RGC binocularity outside the special case of the retinohypothalamic tract (Magnin et al., 1989; Fernandez et al., 2016).

Cck-Cre Brn3c^{CKOAP/+} mice label tSbC RGCs throughout postnatal development

To analyze how tSbC RGCs establish target- and layer-specific axonal projections, we first needed to test whether *Cck-Cre Brn3c^{CKOAP/+}* mice selectively label these cells during development. We prepared retinal whole mounts from P0, P5, P10, P15, and P20 mice to address this question. At P0, some alkaline-phosphatase-expressing postmitotic RGCs have not yet retracted their apical processes and completed migration to the ganglion cell layer (Sajgo et al., 2016; Fig. 4A); at all other

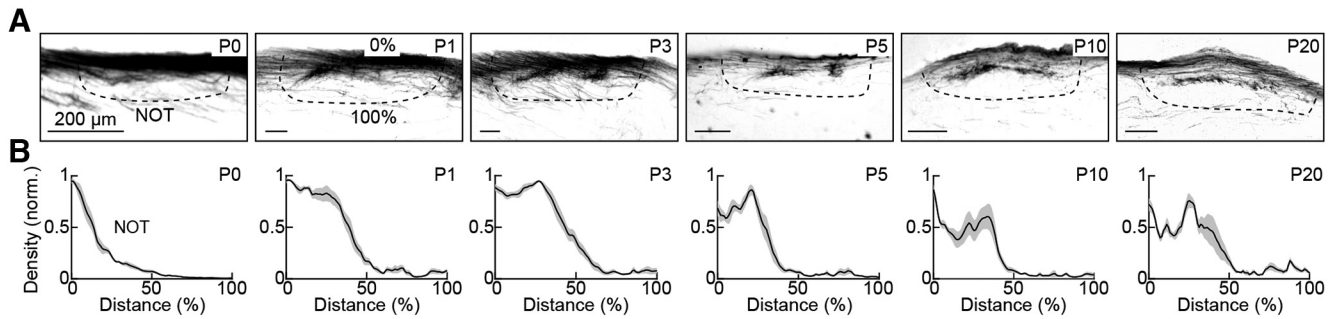


Figure 9. Development of the tSbC RGCs NOT innervation. **A**, Developmental time series of coronal sections through the NOT of *Cck-Cre Brn3c^{CKOAP/+}* mice (P0, P1, P3, P5, P10, P20, from left to right). **B**, Labeling profiles from the optic tract (0%) to the caudomedial margin of NOT (100%) across development (P0, P1, P3, P5, P10, P20, from left to right). Lines indicate the mean, and shaded areas indicate SEM ($n = 3-5$ mice at each time point).

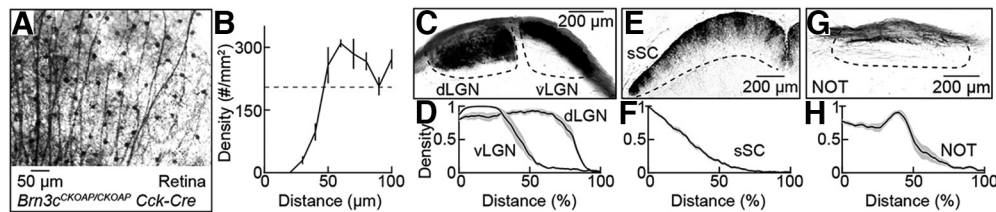


Figure 10. tSbC RGC mosaics and axonal projections develop independently of *Brn3c*. **A**, Except of a P30 *Cck-Cre Brn3c^{CKOAP/CKOAP}* retina showing alkaline phosphatase expression in the tSbC RGC mosaic. **B**, DRP of RGCs labeled in P30 *Cck-Cre Brn3c^{CKOAP/CKOAP}* mice ($n = 5$ retinas). **C, E, G**, Coronal sections of the LGN complex (**C**), SC (**E**), and NOT (**G**). **D, F, H**, Labeling profiles from the optic tract (0%) to the medial boundaries of dLGN and vLGN (**D**, 100%), the surface of SC (0%) to the caudal margin of sSC (**F**, 100%), and the optic tract (0%) to the caudomedial margin of NOT (**H**, 100%). Lines indicate the mean, and shaded areas indicate SEM ($n = 3$ mice).

ages, labeling was restricted to the ganglion cell layer (Fig. 4B–E). The density of labeled RGCs increased with age (P0, 96 ± 8 cells/mm²; P5, 109 ± 12 cells/mm²; P10, 130 ± 8 cells/mm²; P15, 171 ± 19 cells/mm²; P20, 215 ± 15 cells/mm²; $n = 10$ retinas for all ages). Most importantly, the RGC DRPs showed clear exclusion zones at all ages (effective radius, P0, 25.7 ± 1.7 μ m; P5, 30.8 ± 1.5 μ m; P10, 30.9 ± 1.4 μ m; P15, 27.7 ± 1.2 μ m; P20, 29.8 ± 1.3 μ m), indicating that *Cck-Cre Brn3c^{CKOAP/+}* mice selectively label tSbC RGCs throughout postnatal development (Fig. 4F–J).

Development of the tSbC RGC projections

We started to study the development of tSbC RGC projections by tracking their innervation of the LGN complex from P0 to P20. At P0 and P1, labeling was restricted to the optic tract with few branches or axon terminals visible in the dLGN or vLGN (Fig. 5A–C). However, by P3, axonal arborizations occupied all but the medial aspect of dLGN and a lateral band of vLGN (Fig. 5A–C). These patterns were maintained to maturity (Fig. 5A–C). We observed no aberrant tSbC RGCs axons in the intergeniculate leaflet at any stage of postnatal development.

We next turned to the SC. Like LGN, tSbC RGC axons had few branches in sSC at P0 and P1 but densely innervated the uppermost layers of sSC by P3, which they continued to occupy at maturity (Fig. 6A–C). We found that neurons in the deeper layers SC (dSC) expressed alkaline phosphatase during early postnatal development (P0 and P5). We confirmed that the sSC labeling reflects tSbC RGC axons entering from the optic tract in sagittal sections (Fig. 7) and through binocular enucleations in developing mice (Fig. 8).

Finally, although tSbC RGC axons were present in the optic tract at P0, we observed few branches in the NOT (Fig. 9A–C). By P3, tSbC RGC axon terminals targeted a narrow band in NOT and maintained this position to maturity (Fig. 9A–C). At

no point in our developmental time series did we find tSbC RGCs axons in other pretectal areas or any retinorecipient targets other than dLGN, vLGN, SC, and SC NOT (Fig. 8). Thus, tSbC RGC axons choose their targets without developmental errors, invade them simultaneously between P1 and P3, and form laminar arborization patterns that are precise from the outset.

tSbC RGC mosaics and axonal projections develop independently of *Brn3*

Brn3 transcription factors contribute to RGC differentiation and terminal identity (Mu and Klein, 2004; Badea et al., 2009). *Brn3a*, *Brn3b*, and *Brn3c* are expressed in multiple RGC types, and their contributions to RGC differentiation and axon targeting have not been studied with cell-type resolution. We generated *Cck-Cre Brn3c^{CKOAP/CKOAP}* mice to explore the influence of *Brn3c* on tSbC RGCs (Badea et al., 2012). We observed no differences in the density of tSbC RGCs (Fig. 9A,B; *Cck-Cre Brn3c^{CKOAP/CKOAP}*, 205 ± 5 cells/mm², $n = 5$ retinas; *Cck-Cre Brn3c^{CKOAP/+}*, 215 ± 15 cells/mm², $n = 10$, $p = 1$, Mann–Whitney *U* test), their mosaic distributions (Fig. 9A,B; exclusion zones, *Cck-Cre Brn3c^{CKOAP/CKOAP}*, 31.7 ± 1.2 μ m, $n = 5$ retinas; *Cck-Cre Brn3c^{CKOAP/+}*, 29.8 ± 1.3 μ m, $n = 10$, $p = 0.21$, Mann–Whitney *U* test), or axonal targeting (Fig. 9C–H), between P20 *Cck-Cre Brn3c^{CKOAP/CKOAP}* and *Cck-Cre Brn3c^{CKOAP/+}* mice. We do not know when in development, *Brn3c* is removed in these mice, but we know that Cre-dependent alkaline phosphatase expression is detectable at least from P0 onward. Thus, the postnatal development of tSbC RGCs and their axonal projections appears to be independent of *Brn3c*.

Discussion

Here, we discover a transgenic intersection (*Cck-Cre* and *Brn3c^{CKOAP}*) that marks a single RGC type in the mouse retina,

the tSbC RGC. Immunohistochemistry (Fig. 1) and single-cell RNA sequencing support the notion that tSbC RGCs coexpress *Cck* and *Brn3c* (Tran et al., 2019; Goetz et al., 2022). We use *Cck-Cre Brn3c^{CKOAP}* mice to map tSbC RGC projections and study their development.

The tSbC RGCs selectively innervate four of the >50 retinorecipient brain areas, dLGN, vLGN, SC, and NOT (Fig. 2). The dLGN and SC are the main image-forming retinal targets (Morin and Studholme, 2014; Martersteck et al., 2017). Both pass information to visual cortex (among other places), dLGN directly to primary visual cortex (V1), and SC via the lateral posterior nucleus of the thalamus to postrhinal cortex (Kerschensteiner and Guido, 2017; Beltramo and Scanziani, 2019; Bennett et al., 2019). SbC responses have been recorded in dLGN, SC, and V1 (Niell and Stryker, 2008; Piscopo et al., 2013; Ito et al., 2017), suggesting that some dLGN and SC neurons receive exclusive or predominant input from tSbC RGCs to relay their signals to visual cortex and other second-order targets. In addition, high-resolution imaging of RGC axon responses suggests that SbC inputs converge with conventional retinal signals onto some dLGN neurons (Liang et al., 2018). The combination of SbC and conventional signals could serve as a contrast gain control mechanism in which SbC signals boost responses to low-contrast stimuli while avoiding response saturation to high-contrast stimuli.

The NOT is part of the accessory optic system, which controls gaze-stabilizing eye movements via the optokinetic reflex arc (Simpson, 1984). The NOT, in particular, mediates ipsiversive horizontal eye movements (Kato et al., 1986; Yakushin et al., 2000; Macé et al., 2018). NOT neuron light responses have, to our knowledge, not been characterized in mice. In rabbits, they are unfailingly direction selective (Colléwijn, 1975). NOT is strongly innervated by ON direction-selective RGCs in rabbits and mice (Pu and Amthor, 1990; Dhande et al., 2013). Thus, it seems likely that tSbC RGCs converge with ON direction-selective RGCs onto NOT neurons, possibly for contrast gain control. It seems less likely that tSbC RGC signals are maintained as a separate information stream in this target. Why tSbC RGCs do not innervate the medial terminal nucleus—the nucleus of the accessory optic system mediating gaze-stabilizing vertical eye movements—is unclear.

The vLGN has recently been shown to mediate influences of light on mood and learning (Huang et al., 2019, 2021). The vLGN also regulates defensive responses to visual threats (Fratzl et al., 2021; Salay and Huberman, 2021), but this regulation appears to be independent of its light responses and retinal input (Fratzl et al., 2021). The vLGN is subdivided into a retinorecipient external (vLGN_e) and a nonretinorecipient internal (vLGN_i) layer. A recent study identified transcriptionally distinct cell types arranged in four sublaminae within vLGN_e (Sabbagh et al., 2020). Our labeling distribution suggests that tSbC RGCs provide input to the outer two layers of vLGN_e (Figs. 2, 5).

The laminar targeting of axons in the other retinorecipient areas suggests that tSbC RGCs provide input to specific circuits in these targets as well. It will be interesting to see whether and where tSbC RGC axons overlap with axons of other SbC RGC types (Jacoby and Schwartz, 2018; Wienbar and Schwartz, 2022). Our discovery of a genetic intersection to target tSbC RGCs should allow us in the future to selectively perturb these cells to clarify their contributions to visual processing and behaviors mediated by the targets identified here.

A previous study found that early-born RGC axons grow along the optic tract prenatally and transiently innervate more targets than they ultimately maintain (Osterhout et al., 2014). In

contrast, late-born RGC axons grow along the optic tract postnatally and make few, if any, targeting errors (Osterhout et al., 2014). We find that tSbC RGC axons span the length of the optic tract at P0, indicating that they grow prenatally. They remain poised there until around P3, when they simultaneously and without error innervate their four targets (Figs. 5–9), revealing further cell-type-specific diversity in the developmental strategies of retinofugal projections.

Some axons of RGCs refine their terminal arbors slowly during postnatal development to attain specific laminar positions in their target areas (Kim et al., 2010; Hong et al., 2014; Osterhout et al., 2014). We find that tSbC RGC axons establish mature lamination patterns shortly after invading their targets (Figs. 5–9). *Brn3* transcription factors are important nodes of the gene regulatory networks that govern RGC differentiation and terminal identity, and *Brn3c* has been suggested to shape axon projection patterns (Wang et al., 2002; Mu and Klein, 2004; Badea et al., 2009). Using cell-type-specific *Brn3c* deletion and axon mapping, we find no difference in the patterns of tSbC RGC axons developing with and without *Brn3c* (Fig. 10). The molecular mechanisms that drive tSbC RGC axon growth keep tSbC RGC axons poised in the optic tract, make them simultaneously invade their targets, and guide them to the correct laminar position, thus, remain unknown. The developmentally stable and selective genetic intersection we identify for tSbC RGC targeting should facilitate future efforts to uncover these mechanisms.

Finally, we find that tSbC RGCs innervate the ipsilateral and the contralateral vLGN and dLGN but only the contralateral SC and NOT (Fig. 3). This could indicate that only a subset of tSbC RGCs innervates SC and NOT or that some tSbC RGC axons bifurcate at the optic chiasm to innervate targets on both sides of the brain. Both options raise interesting developmental and molecular questions and could be distinguished using single-cell labeling approaches in future studies (Hong et al., 2011; Fernandez et al., 2016; Herrera et al., 2019; Mason and Slavi, 2020).

References

- Badea TC, Wang Y, Nathans J (2003) A noninvasive genetic/pharmacologic strategy for visualizing cell morphology and clonal relationships in the mouse. *J Neurosci* 23:2314–2322.
- Badea TC, Cahill H, Ecker J, Hattar S, Nathans J (2009) Distinct roles of transcription factors *brn3a* and *brn3b* in controlling the development, morphology, and function of retinal ganglion cells. *Neuron* 61:852–864.
- Badea TC, Nathans J (2011) Morphologies of mouse retinal ganglion cells expressing transcription factors *Brn3a*, *Brn3b*, and *Brn3c*: analysis of wild type and mutant cells using genetically-directed sparse labeling. *Vision Res* 51:269–279.
- Badea TC, Williams J, Smallwood P, Shi M, Motajo O, Nathans J (2012) Combinatorial expression of *Brn3* transcription factors in somatosensory neurons: genetic and morphologic analysis. *J Neurosci* 32:995–1007.
- Baden T, Berens P, Franke K, Román Rosón M, Bethge M, Euler T (2016) The functional diversity of retinal ganglion cells in the mouse. *Nature* 529:345–350.
- Bae JA, Mu S, Kim JS, Turner NL, Tartavull I, Kemnitz N, Jordan CS, Norton AD, Silversmith WM, Prentki R, Sorek M, David C, Jones DL, Bland D, Sterling ALR, Park J, Briggman KL, Seung HS (2018) Digital museum of retinal ganglion cells with dense anatomy and physiology. *Cell* 173:1293–1306.e19.
- Beltramo R, Scanziani M (2019) A collicular visual cortex: neocortical space for an ancient midbrain visual structure. *Science* 363:64–69.
- Bennett C, Gale SD, Garrett ME, Newton ML, Callaway EM, Murphy GJ, Olsen SR (2019) Higher-order thalamic circuits channel parallel streams of visual information in mice. *Neuron* 102:477–492.e5.
- Cai D, Cohen KB, Luo T, Lichtman JW, Sanes JR (2013) Improved tools for the Brainbow toolbox. *Nat Methods* 10:540–547.

- Collewijn H (1975) Direction-selective units in the rabbit's nucleus of the optic tract. *Brain Res* 100:489–508.
- de Monasterio FM (1978) Properties of ganglion cells with atypical receptive-field organization in retina of macaques. *J Neurophysiol* 41:1435–1449.
- Dhande OS, Estevez ME, Quattrochi LE, El-Danaf RN, Nguyen PL, Berson DM, Huberman AD (2013) Genetic dissection of retinal inputs to brain-stem nuclei controlling image stabilization. *J Neurosci* 33:17797–17813.
- Dräger UC, Olsen JF (1980) Origins of crossed and uncrossed retinal projections in pigmented and albino mice. *J Comp Neurol* 191:383–412.
- Erskine L, Herrera E (2007) The retinal ganglion cell axon's journey: insights into molecular mechanisms of axon guidance. *Dev Biol* 308:1–14.
- Fernandez DC, Chang Y-T, Hattar S, Chen S-K (2016) Architecture of retinal projections to the central circadian pacemaker. *Proc Natl Acad Sci U S A* 113:6047–6052.
- Fratzl A, Koltchev AM, Vissers N, Tan YL, Marques-Smith A, Vanessa Stempel A, Branco T, Hofer SB (2021) Flexible inhibitory control of visually evoked defensive behavior by the ventral lateral geniculate nucleus. *Neuron* 109:3810–3822.e9.
- Goetz J, Jessen ZF, Jacobi A, Mani A, Cooler S, Greer D, Kadri S, Segal J, Shekhar K, Sanes JR, Schwartz G (2022) Unified classification of mouse retinal ganglion cells using function, morphology, and gene expression. *Cell Rep* 40:111040.
- Gollisch T, Meister M (2010) Eye smarter than scientists believed: neural computations in circuits of the retina. *Neuron* 65:150–164.
- Hattar S, Kumar M, Park A, Tong P, Tung J, Yau K-W, Berson DM (2006) Central projections of melanopsin-expressing retinal ganglion cells in the mouse. *J Comp Neurol* 497:326–349.
- Herrera E, Erskine L, Morenilla-Palao C (2019) Guidance of retinal axons in mammals. *Semin Cell Dev Biol* 85:48–59.
- Hong YK, Kim I-J, Sanes JR (2011) Stereotyped axonal arbors of retinal ganglion cell subsets in the mouse superior colliculus. *J Comp Neurol* 519:1691–1711.
- Hong YK, Park S, Litvina EY, Morales J, Sanes JR, Chen C (2014) Refinement of the retinogeniculate synapse by bouton clustering. *Neuron* 84:332–339.
- Huang L, Xi Y, Peng Y, Yang Y, Huang X, Fu Y, Tao Q, Xiao J, Yuan T, An K, Zhao H, Pu M, Xu F, Xue T, Luo M, So K-F, Ren C (2019) A visual circuit related to habenula underlies the antidepressive effects of light therapy. *Neuron* 102:128–142.e8.
- Huang X, Huang P, Huang L, Hu Z, Liu X, Shen J, Xi Y, Yang Y, Fu Y, Tao Q, Lin S, Xu A, Xu F, Xue T, So K-F, Li H, Ren C (2021) A visual circuit related to the nucleus reuniens for the spatial-memory-promoting effects of light treatment. *Neuron* 109:347–362.e7.
- Huberman AD, Manu M, Koch SM, Susman MW, Lutz AB, Ullian EM, Baccus SA, Barres BA (2008) Architecture and activity-mediated refinement of axonal projections from a mosaic of genetically identified retinal ganglion cells. *Neuron* 59:425–438.
- Huberman AD, Wei W, Elstrott J, Stafford BK, Feller MB, Barres BA (2009) Genetic identification of an On-Off direction-selective retinal ganglion cell subtype reveals a layer-specific subcortical map of posterior motion. *Neuron* 62:327–334.
- Ito S, Feldheim DA, Litke AM (2017) Segregation of visual response properties in the mouse superior colliculus and their modulation during locomotion. *J Neurosci* 37:8428–8443.
- Jacoby J, Schwartz GW (2018) Typology and circuitry of suppressed-by-contrast retinal ganglion cells. *Front Cell Neurosci* 12:269.
- Jacoby J, Zhu Y, DeVries SH, Schwartz GW (2015) An amacrine cell circuit for signaling steady illumination in the retina. *Cell Rep* 13:2663–2670.
- Johnson KP, Fitzpatrick MJ, Zhao L, Wang B, McCracken S, Williams PR, Kerschensteiner D (2021) Cell-type-specific binocular vision guides predation in mice. *Neuron* 109:1527–1539.e4.
- Kato I, Harada K, Hasegawa T, Igarashi T, Koike Y, Kawasaki T (1986) Role of the nucleus of the optic tract in monkeys in relation to optokinetic nystagmus. *Brain Res* 364:12–22.
- Kerschensteiner D (2022) Feature detection by retinal ganglion cells. *Annu Rev Vis Sci*. Online advance publication. Retrieved August 9, 2022. doi: 10.1146/annurev-vision-100419-112009.
- Kerschensteiner D, Guido W (2017) Organization of the dorsal lateral geniculate nucleus in the mouse. *Vis Neurosci* 34:E008.
- Kim I-J, Zhang Y, Yamagata M, Meister M, Sanes JR (2008) Molecular identification of a retinal cell type that responds to upward motion. *Nature* 452:478–482.
- Kim I-J, Zhang Y, Meister M, Sanes JR (2010) Laminar restriction of retinal ganglion cell dendrites and axons: subtype-specific developmental patterns revealed with transgenic markers. *J Neurosci* 30:1452–1462.
- Knöferle J, Koch JC, Ostendorf T, Michel U, Planchamp V, Vutova P, Tönges L, Stadelmann C, Brück W, Bähr M, Lingor P (2010) Mechanisms of acute axonal degeneration in the optic nerve in vivo. *Proc Natl Acad Sci U S A* 107:6064–6069.
- Levick WR (1967) Receptive fields and trigger features of ganglion cells in the visual streak of the rabbits retina. *J Physiol* 188:285–307.
- Liang L, Fratzl A, Goldey G, Ramesh RN, Sugden AU, Morgan JL, Chen C, Andermann ML (2018) A fine-scale functional logic to convergence from retina to thalamus. *Cell* 173:1343–1355.e24.
- Macé É, Montaldo G, Trenholm S, Cowan C, Brignall A, Urban A, Roska B (2018) Whole-brain functional ultrasound imaging reveals brain modules for visuomotor integration. *Neuron* 100:1241–1251.e7.
- Madisen L, Zwingman TA, Sunkin SM, Oh SW, Zariwala HA, Gu H, Ng LL, Palmiter RD, Hawrylycz MJ, Jones AR, Lein ES, Zeng H (2010) A robust and high-throughput Cre reporting and characterization system for the whole mouse brain. *Nat Neurosci* 13:133–140.
- Magnin M, Cooper HM, Mick G (1989) Retinohypothalamic pathway: a breach in the law of Newton–Müller–Gudden? *Brain Res* 488:390–397.
- Martersteck EM, Hirokawa KE, Evarts M, Bernard A, Duan X, Li Y, Ng L, Oh SW, Ouellette B, Royall JJ, Stoecklin M, Wang Q, Zeng H, Sanes JR, Harris JA (2017) Diverse central projection patterns of retinal ganglion cells. *Cell Rep* 18:2058–2072.
- Masland RH, Martin PR (2007) The unsolved mystery of vision. *Curr Biol* 17:R577–82.
- Mason C, Slavi N (2020) Retinal ganglion cell axon wiring establishing the binocular circuit. *Annu Rev Vis Sci* 6:215–236.
- Moore DL, Goldberg JL (2011) Multiple transcription factor families regulate axon growth and regeneration. *Dev Neurobiol* 71:1186–1211.
- Morin LP, Studholme KM (2014) Retinofugal projections in the mouse. *J Comp Neurol* 522:3733–3753.
- Mu X, Klein WH (2004) A gene regulatory hierarchy for retinal ganglion cell specification and differentiation. *Semin Cell Dev Biol* 15:115–123.
- Niell CM, Stryker MP (2008) Highly selective receptive fields in mouse visual cortex. *J Neurosci* 28:7520–7536.
- Osterhout JA, Josten N, Yamada J, Pan F, Wu S-W, Nguyen PL, Panagiotakos G, Inoue YU, Egusa SF, Volgyi B, Inoue T, Bloomfield SA, Barres BA, Berson DM, Feldheim DA, Huberman AD (2011) Cadherin-6 mediates axon-target matching in a non-image-forming visual circuit. *Neuron* 71:632–639.
- Osterhout JA, El-Danaf RN, Nguyen PL, Huberman AD (2014) Birthdate and outgrowth timing predict cellular mechanisms of axon target matching in the developing visual pathway. *Cell Rep* 8:1006–1017.
- Osterhout JA, Stafford BK, Nguyen PL, Yoshihara Y, Huberman AD (2015) Contactin-4 mediates axon-target specificity and functional development of the accessory optic system. *Neuron* 86:985–999.
- Parmhans N, Sajjo S, Niu J, Luo W, Badea TC (2018) Characterization of retinal ganglion cell, horizontal cell, and amacrine cell types expressing the neurotrophic receptor tyrosine kinase Ret. *J Comp Neurol* 526:742–766.
- Parmhans N, Fuller AD, Nguyen E, Chuang K, Swygart D, Wienbar SR, Lin T, Kozmik Z, Dong L, Schwartz GW, Badea TC (2021) Identification of retinal ganglion cell types and brain nuclei expressing the transcription factor *Brn3c/Pou4f3* using a Cre recombinase knock-in allele. *J Comp Neurol* 529:1926–1953.
- Piscopo DM, El-Danaf RN, Huberman AD, Niell CM (2013) Diverse visual features encoded in mouse lateral geniculate nucleus. *J Neurosci* 33:4642–4656.
- Pu ML, Amthor FR (1990) Dendritic morphologies of retinal ganglion cells projecting to the nucleus of the optic tract in the rabbit. *J Comp Neurol* 302:657–674.
- Reese BE (1988) “Hidden lamination” in the dorsal lateral geniculate nucleus: the functional organization of this thalamic region in the rat. *Brain Res* 472:119–137.
- Rheume BA, Jereen A, Bolisetty M, Sajid MS, Yang Y, Renna K, Sun L, Robson P, Trakhtenberg EF (2018) Single cell transcriptome profiling of retinal ganglion cells identifies cellular subtypes. *Nat Commun* 9:2759.
- Rodieck RW (1967) Receptive fields in the cat retina: a new type. *Science* 157:90–92.
- Rodieck RW (1991) The density recovery profile: a method for the analysis of points in the plane applicable to retinal studies. *Vis Neurosci* 6:95–111.

- Sabbagh U, Govindaiah G, Somaiya RD, Ha RV, Wei JC, Guido W, Fox MA (2020) Diverse GABAergic neurons organize into subtype-specific sublaminae in the ventral lateral geniculate nucleus. *J Neurochem* 159:479–497.
- Sajgo S, Ali S, Popescu O, Badea TC (2016) Dynamic expression of transcription factor Brn3b during mouse cranial nerve development. *J Comp Neurol* 524:1033–1061.
- Salay LD, Huberman AD (2021) Divergent outputs of the ventral lateral geniculate nucleus mediate visually evoked defensive behaviors. *Cell Rep* 37:109792.
- Schindelin J, Arganda-Carreras I, Frise E, Kaynig V, Longair M, Pietzsch T, Preibisch S, Rueden C, Saalfeld S, Schmid B, Tinevez J-Y, White DJ, Hartenstein V, Eliceiri K, Tomancak P, Cardona A (2012) Fiji: an open-source platform for biological-image analysis. *Nat Methods* 9:676–682.
- Shi M, Kumar SR, Motajo O, Kretschmer F, Mu X, Badea TC (2013) Genetic interactions between Brn3 transcription factors in retinal ganglion cell type specification. *PLoS One* 8:e76347.
- Simpson JI (1984) The accessory optic system. *Annu Rev Neurosci* 7:13–41.
- Sivyer B, Taylor WR, Vaney DI (2010) Uniformity detector retinal ganglion cells fire complex spikes and receive only light-evoked inhibition. *Proc Natl Acad Sci U S A* 107:5628–5633.
- Soto F, Watkins KL, Johnson RE, Schottler F, Kerschensteiner D (2013) NGL-2 regulates pathway-specific neurite growth and lamination, synapse formation, and signal transmission in the retina. *J Neurosci* 33:11949–11959.
- Su J, Sabbagh U, Liang Y, Olejníková L, Dixon KG, Russell AL, Chen J, Pan YA, Triplett JW, Fox MA (2021) A cell-ECM mechanism for connecting the ipsilateral eye to the brain. *Proc Natl Acad Sci U S A* 118:2104343118.
- Taniguchi H, He M, Wu P, Kim S, Paik R, Sugino K, Kvitsani D, Kvitsani D, Fu Y, Lu J, Lin Y, Miyoshi G, Shima Y, Fishell G, Nelson SB, Huang ZJ (2011) A resource of Cre driver lines for genetic targeting of GABAergic neurons in cerebral cortex. *Neuron* 71:995–1013.
- Tien N-W, Pearson JT, Heller CR, Demas J, Kerschensteiner D (2015) Genetically identified suppressed-by-contrast retinal ganglion cells reliably signal self-generated visual stimuli. *J Neurosci* 35:10815–10820.
- Tran NM, Shekhar K, Whitney IE, Jacobi A, Benhar I, Hong G, Yan W, Adiconis X, Arnold ME, Lee JM, Levin JZ, Lin D, Wang C, Lieber CM, Regev A, He Z, Sanes JR (2019) Single-cell profiles of retinal ganglion cells differing in resilience to injury reveal neuroprotective genes. *Neuron* 104:1039–1055.e12.
- Wang SW, Mu X, Bowers WJ, Kim D-S, Plas DJ, Crair MC, Federoff HJ, Gan L, Klein WH (2002) Brn3b/Brn3c double knockout mice reveal an unsuspected role for Brn3c in retinal ganglion cell axon outgrowth. *Development* 129:467–477.
- Wienbar S, Schwartz GW (2022) Differences in spike generation instead of synaptic inputs determine the feature selectivity of two retinal cell types. *Neuron* 110:2110–2123.e4.
- Williams PR, Benowitz LI, Goldberg JL, He Z (2020) Axon regeneration in the mammalian optic nerve. *Annu Rev Vis Sci* 6:195–213.
- Xiang M, Zhou L, Macke JP, Yoshioka T, Hendry SH, Eddy RL, Shows TB, Nathans J (1995) The Brn-3 family of POU-domain factors: primary structure, binding specificity, and expression in subsets of retinal ganglion cells and somatosensory neurons. *J Neurosci* 15:4762–4785.
- Yakushin SB, Gizzi M, Reisine H, Raphan T, Büttner-Ennever J, Cohen B (2000) Functions of the nucleus of the optic tract (NOT). II. Control of ocular pursuit. *Exp Brain Res* 131:433–447.
- Yonehara K, Shintani T, Suzuki R, Sakuta H, Takeuchi Y, Nakamura-Yonehara K, Noda M (2008) Expression of SPIG1 reveals development of a retinal ganglion cell subtype projecting to the medial terminal nucleus in the mouse. *PLoS One* 3:e1533.